LA-UR- 09-05234

Approved for public release; distribution is unlimited.

Title: Review of Proton Radiography at LANSCE

Author(s): Frank Merrill for the pRad Collabortion

Intended for: NNSA

Los Alamos
NATIONAL LABORATORY
EST. 1943

Los Alamos National Laboratory, an affirmative action/equal opportunity employer, is operated by the Los Alamos National Security, LLC for the National Nuclear Security Administration of the U.S. Department of Energy under contract DE-AC52-06NA25396. By acceptance of this article, the publisher recognizes that the U.S. Government retains a nonexclusive, royalty-free license to publish or reproduce the published form of this contribution, or to allow others to do so, for U.S. Government purposes. Los Alamos National Laboratory requests that the publisher identify this article as work performed under the auspices of the U.S. Department of Energy. Los Alamos National Laboratory strongly supports academic freedom and a researcher's right to publish; as an institution, however, the Laboratory does not endorse the viewpoint of a publication or guarantee its technical correctness.

Form 836 (7/06)

Review of Proton Radiography at LANSCE

Introduction

Until recently, the experimental tools to observe the dynamic behavior of materials when driven by high explosives had not changed much since the earliest days of the nuclear weapons program. At the same time the need to develop predictive models of material behavior under such conditions had grown substantially, especially after the cessation of U.S. nuclear testing in 1989. Over the last decade, a new imaging technique has been developed that uses high-energy protons, rather than x-rays, to radiograph materials during dynamic experiments. Proton radiography allows researchers to make short movies and obtain much more detailed information on the motions and densities of materials when driven by shock compression than was ever possible before. The penetrating power, or long mean free path, of protons and the ability to focus them are opening up new opportunities for quantitative experiments, accurate model development, and designer training that will revolutionize how the U.S. nuclear stockpile is stewarded in the future.

Capabilities of the Proton Radiography (pRad) Program

The proton radiography program at Los Alamos occurs in the Line C Experimental Area at the Los Alamos Neutron Science Center (LANSCE). The proton radiography program is capable of taking a series of 31 images of a dynamic event. The spatial resolution of the large field-of-view system (120 mm field of view) is 180 μm. A newer X3 magnifier system provides higher resolution, 75 μm, over a smaller field-of-view (40 mm). The maximum density that can be measured with 800 MeV protons is 70 g/cc. In addition to the time-resolved imaging and density measurements available with pRad, other diagnostics such as VISAR, PDV (both surface-velocity measurements), and timing pins are available. New capabilities also include controlled heating and cooling of shots, as well as a 1-D powder gun driver. New capabilities such as optical imaging are anticipated within the next year.

High-energy proton beams serve as an almost ideal radiographic probe for studying the physics of nuclear weapons because their mean free path (or average distance traveled between collisions) can be tailored to see inside almost any experiment. Protons are charged particles that bend as they move through magnetic fields, so they can be focused by magnetic lenses. The contrast in an experiment can then be optimized with different collimators. It is this feature that has enabled the pRad program at LANSCE to address many different physics problems with the same proton beam energy.

There have been over 300 dynamic experiments performed since the pRad effort began a decade ago. Currently, about 40 dynamic experiments are performed each year. Two-thirds of these experiments are related to weapons physics, and the other third are designed to study specific weapons engineering issues or to enhance the measurement capabilities at Line C.

Validation and Verification

In order to simulate the implosion of a nuclear weapon accurately, with understanding of errors, we need to model the physics of explosive detonation and burn front propagation and the dynamic behavior of metals under explosive loading. In a weapon, materials exhibit behaviors at extremely high strain rates. This results in detonations at high pressures, metals fracturing under high loads, and metals undergoing "spall," or fracturing inside the metal caused by shock loading. Sometimes these behaviors are studied in an integral way using hydrotests. Often, however, theoreticians and numerical physicists would like to understand specific physical behaviors under very controlled experimental conditions. In order to improve their models and simulations, and quantify uncertainties, they need experimental data with high spatial and temporal resolution.

Proton radiography is a very valuable tool for understanding weapons physics. There are several diagnostic tools developed to assess hydrodynamic behavior, however, most rely on surface measurements and are unable to interrogate the critical state variables and stress-strain response in the interior of the hydro-components. Modeling depends on accurately capturing the time evolution of those state variables and stress-strain responses on a microsecond time scale. Proton radiography, with its ability to penetrate and accurately image the interior of highly compressed components, as well as its highly flexible and precisely recordable pulsed format, is uniquely suited to providing the necessary data for weapon certification codes and models.

Proton radiography at LANL is being used to perform classified and unclassified experiments relating to equation-of-state for high explosives (HE) and materials, damage and fracture, material properties of explosives, and hydrodynamics and mix. As an example in 2005, 38 dynamic experiments were performed at Line C. There were twelve damage/spall experiments and high-explosive cookoff experiments that were performed in order to support the ASC Validation and Verification efforts at Los Alamos by providing scientific data to help validate and calibrate fracture and HE equation-of-state (EOS) models. The cookoff experiments also created a new capability at Line C to study the time evolution of heated HE and to trigger its eventual detonation. Nineteen classified experiments were performed using pRad to study specific engineering issues (for Sandia National Laboratory), and for validation of ASC weapons simulations. The final seven experiments performed last year added the powder gun capability to pRad. With the powder gun, we can now study equation of state of shock-loaded materials under well-controlled conditions that will improve our understanding of the EOS of poorly-understood metals such as tin and iron.

1. High explosive equation of state and dynamic material properties:
Cookoff experiments, PI: Laura Smilowitz, CHEM-PCAS, Physical Chemistry and Applied Spectroscopy

High explosives are usually initiated with detonators, but it is important to understand the properties of explosives as they are heated, and when the temperature is large enough to cause a thermal explosion. The understanding of thermal explosions has been hindered compared to that of detonations by the difficulty of predicting the exact time of the event. A technique such as proton radiography can illuminate the events at the center of a thermal explosion but requires the ability to control ignition time to within a hundred microseconds. A technique for synchronizing a thermal explosion at the center of a heated explosive with hundred-microsecond accuracy at the end of a several hours of heating has been developed. Technical accomplishments to achieve this included controlling the location of ignition and measuring the temperature at the ignition location. Once thermal runaway begins, synchronization is achieved by using a fiber-coupled laser to provide a temperature perturbation within the ignition volume. Using a convergent heating geometry and carefully chosen heat profile to determine the ignition location and then embedding a fiber optic at that location to provide the temperature jump using a free running YAG, we were able to field this experiment at the pRad facility at LANSCE and image the onset of burning in the explosive and subsequent case expansion. This allows us to better understand thermal explosion and opens up the field of thermal explosion research to diagnostics previously inaccessible.

The quasi-static images taken during heating show the volume expansion from the phase change is accommodated in the shot (see Figure 1). From the dynamic images at ignition, we are able to put together a model for burn propagation that includes cracking, convection, and conductive consumption of material.

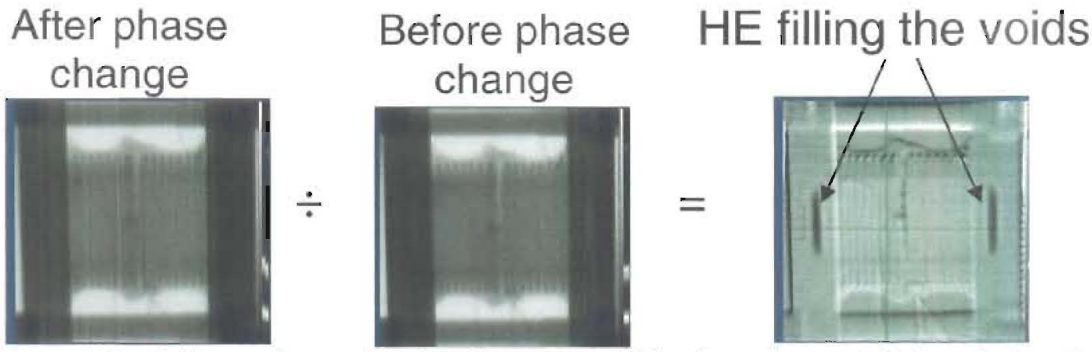

Figure 1. Cookoff experiments showing phase measurable phase change of high explosives during heating.

The thermal explosion appears to originate at a hot spot and quickly propagates though cracks in the material. The material between the cracks then reacts more slowly. This can be observed in sequence of radiographs shown in Figure 2. These are a composite of two experiments showing the initiation of the reaction of the high explosive. The relative off set in time has been established by looking at the metal motion in later time data.

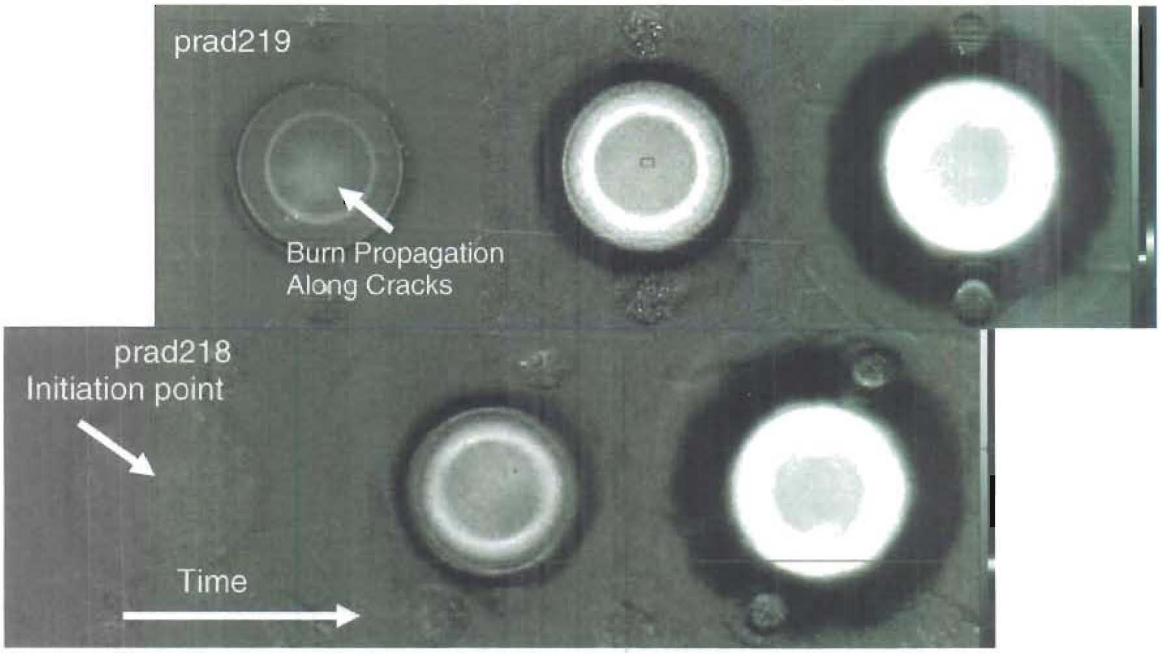

Figure 2. Cookoff experiments showing initiation of heated high explosives along cracks.

Figure 3 shows the Proton transmission recorded along a diameter in the radial view. The data are normalized to 1 for transmission through the initial solid explosive and vertically offset to display proton transmission at different times. Data from a sequence of 13 images are shown at 14 μs intervals starting at 2 μs subsequent to ignition. The solid lines are calculations of normalized density using a model of convective propagation of ignition and consumption by conductive burning.

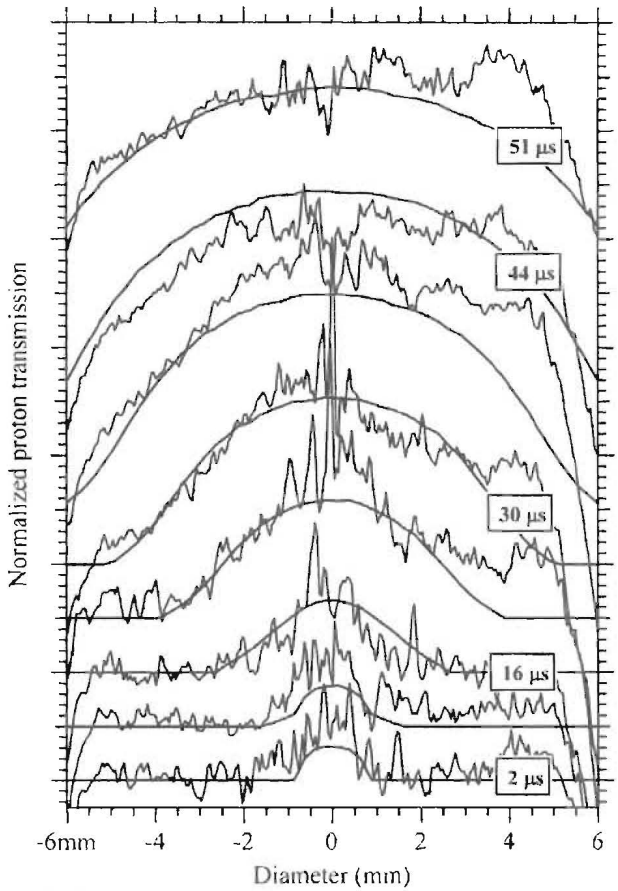

Figure 3: Proton transmission recorded along a diameter in the radial view. The solid lines are calculations of normalized density using a model of convective propagation of ignition and consumption by conductive burning.

This data was published in Physical Review Letters (PRL **100,** 228301 2008).

2. Dynamic material failure and fracture:
Depleted Uranium Hemispherical Shell Experiments, PI: Larry Hull, EHT-H, Hydrodynamics; Calculations: Mark Potocki, X-2-PC, Predictive Capability.

Simulation of material thinning and breakup under combined loading conditions has presented many modeling and numerical challenges. Experiments were designed to show the evolution of depleted uranium fracture in a thin, hemispherical geometry. Proton radiography provides a time history of material failure that can be directly compared to the models implemented in ASC codes. As shown in Figure 3, the fracture of depleted uranium poses a stringent challenge to fracture models, and the time evolution and spatial distribution of material must be matched to the simulations. The metrics for comparison with simulations are onset of damage, open crack area, and extent of area partially shaded by material.

The entire pRad experiment was simulated in two-dimensions, from detonation to late time, using both the P_{min} and TEPLA models. New analysis techniques were developed to provide quantitative comparisons between experimental and simulated radiographs by calculating the material distribution along any ray in the images from early to late time (reference figure). These techniques showed excellent agreement (within 3%) between the amount of open area, area with uranium, and areas with intermediate intensity levels. These quantitative methods were used to perform mesh refinement and time step refinement studies to test the convergence of the simulations. Work on analysis of the experimental data is still ongoing, and new three-dimensional simulations are being run.

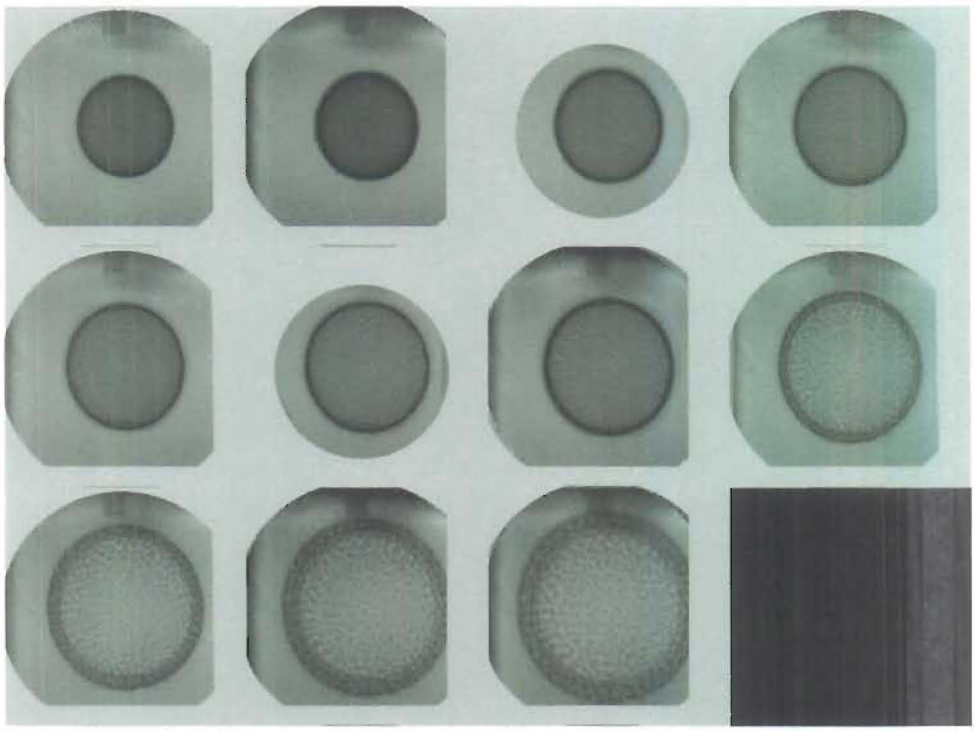

Figure 3. A time series of proton radiographs of an expanding hemi-shell of depleted uranium showing the shear band fracture into "corn flakes."

Proton radiograph images showed the onset of damage in less than 3μs after the shock front reached the inner surface of the U6Nb hemisphere. Simulations using P_{min} show no damage in this time, but the TEPLA simulations show significant deviations in density, although none of the deviations are completely through the thickness of the shell. Later time simulations, shown in Figure 4, illustrate how the P_{min} model fails to capture the fracture of the material.

Quantification of simulations is possible by comparing the intensity of the image generated experimentally and a synthetic radiograph generated by rotating the 2-D simulation, as shown on the left in Figure 5. The rays shown in Figure 5 indicate areas where quantitative comparisons were made. This method, still under development, demonstrates that the relative areas fully open, partially obscured, and fully covered by fragments as observed are simulated in 2-D using TEPLA with high precision. The pRad experimental data have provided highly resolved temporal and spatial data for validation of the implementation of a damage model in a LANL ASC code.

The hemi-shell experimental series was also used to put upper and lower limits on the density of the material that is in between the large chunks of metal, called fines. Figure 6 shows the areal density estimates of the fines in the depleted uranium experiments. No other measurement technique has the resolution to measure, directly or indirectly, the density of the fines.

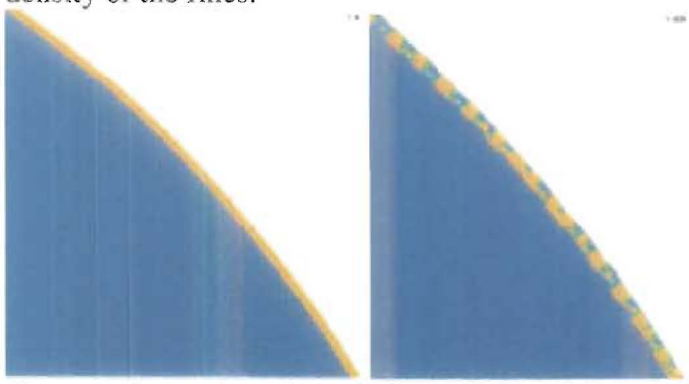

Figure 4. Comparison of simulations of U6Nb shell explosively driven, at 14.0 μs. On the left is a simulation using Pmin. On the right is a simulation using TEPLA. The TEPLA simulation predicts significant density loss through much of the shell, while the Pmin simulation predicts no shell breakup.

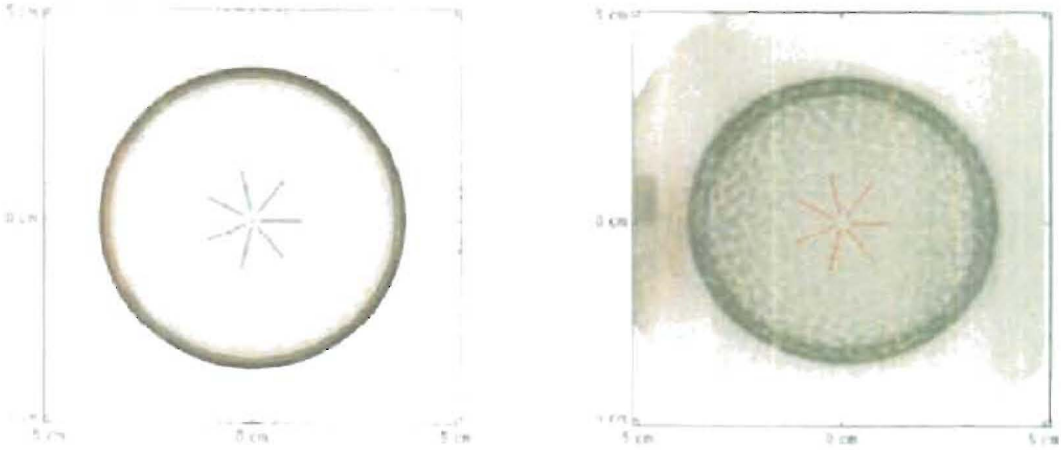

Figure 5. Comparison of 2-D simulation obtained using TEPLA/PTW of explosively-driven 40mm hemisphere, rotated to enable comparison of the proton radiograph taken 14.0 μs after detonation. The lines drawn on the figures were used to evaluate comparative densities.

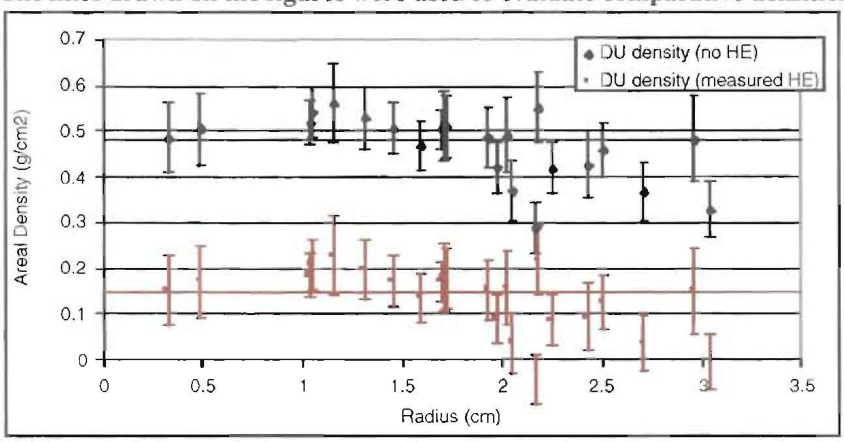

Figure 6. Upper and lower areal density limits on material within the cracks of a fracturing depleted uranium hemi-shell.

3. Material damage caused by spall:
Spall experiments, PI: David Holtkamp, PHY-HXP, Hydrodynamics & X-ray Physics; Calculations: Michael Prime, WT-SD, Structural Dynamics.

Along with fracture, materials can fail due to spall, where high strain inside the metal causes it to rupture internally. Proton radiography provides a time evolution of the internal material failure mechanisms that characterize spall damage. In the past, models have only been tested by matching the velocity of the outer surface of the failing material. This limited experimental information is not enough to constrain the models. A series of pRad experiments examined failure in copper, aluminum, tantalum, tin, and other materials. Figure shows proton radiographs of the spall failure in these materials at late times. Each material clearly exhibits distinct properties under spall conditions that test both the EOS and failure models for the materials. It is challenging to use the same ASC code to capture the stiff spall layers of tantalum, while also capturing the melting of tin.

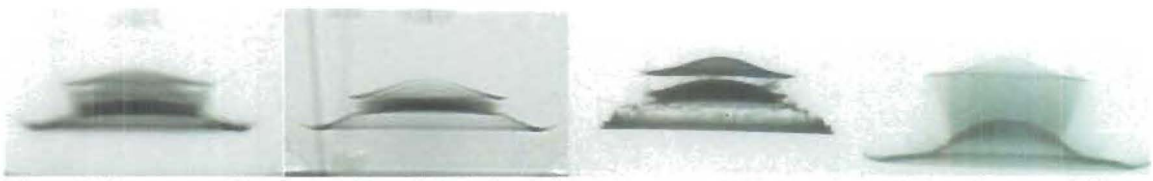

Figure 1. Proton radiographs of spall in (left to right) Copper, 6061 Aluminum, Tantalum, and Tin.

Under some conditions, tin will melt, but under others it spalls without melting. Proton radiography can capture the different properties of tin under both of these conditions and provide data needed to test the modeling of these failure modes.

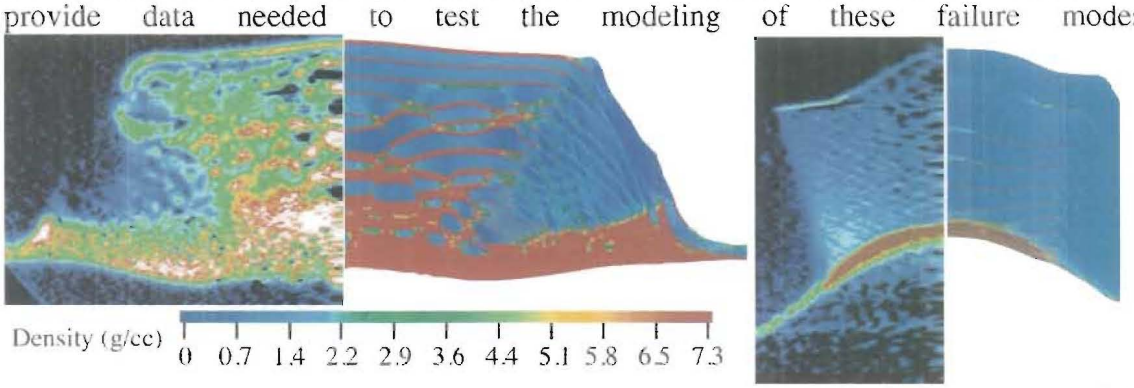

Figure shows comparisons between calculation and experiment for two types of tin experiments. The first, where the tin does not melt, and the second, where the tin does. The shots had varying metal thicknesses, which led to different metal pressures and different melt and spall behavior.

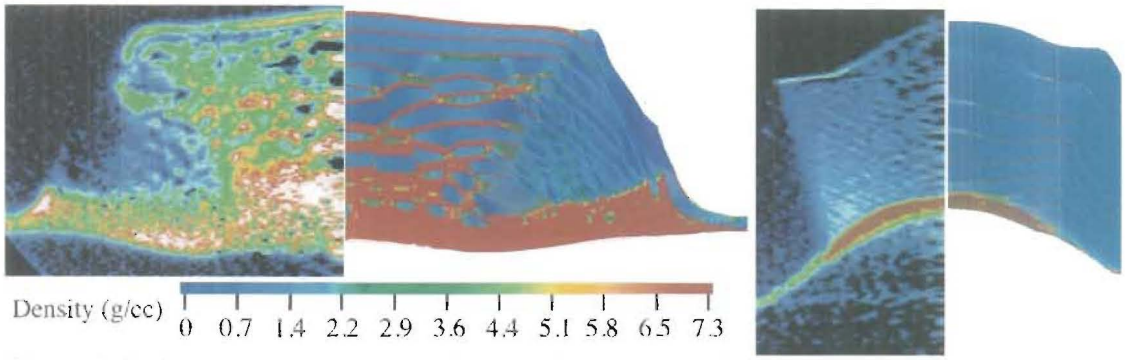

Figure 2. Left, experiment and simulation of the failure of a tin disk due to spall (unmelted); Right, tin that has melted upon spall. Proton radiographs show the Abel inverted volume density field, which allows direct comparison to the calculated density field.

The radiographic data were used to calibrate and validate both the Lindemann melt law and P_{min} failure model. Such melt behavior under high-explosive loading is a crucial prediction capability, but it is very difficult to find experimental data that reveal enough physics to truly exercise any model. The pRad tin data proved uniquely capable to allow the comparison and give the intuitive understanding of the evolving physical process and the performance of the computational model. The copper and tantalum pRad data are currently being used to test the TEPLA failure model.

4. Material equation-of-state under shock loading:

Powder Gun Experiments, PI: Paolo Rigg, DE-9 Cynthia Schwartz, P-25

The results of a series of dynamic experiments were published in late 2008 demonstrating the ability of 800 MeV proton radiography to directly measure points on the Hugoniot with <1% dynamic density errors (PHYSICAL REVIEW B 77, 220101 R 2008). These were the results of proof of principle experiments, placing points on the Hugoniot of well known materials, copper and aluminum, see table 1 and figure 1

TABLE I. Summary of the experiments with the uncertainties for each quantity shown in parentheses.

Experiment	Impactor/ sample	Impactor velocity (mm/μs)	Peak stress (GPa)	Initial density (g/cm³)	Calculated density (g/cm³)	Measured density (g/cm³)	Agreement
1	Al 6061 T6	1.452	12.27	2.710	3.067	3.070	0.1%
		(0.012)	(0.11)	(0.003)	(0.005)	(0.025)	
2	Al 6061-T6	1.422	11.98	2.710	3.060	3.056	0.1%
		(0.002)	(0.03)	(0.003)	(0.004)	(0.020)	
3	OFHC Cu	1.30	28.59	8.928	10.30	10.28	0.2%
		(0.04)	(0.91)	(0.003)	(0.05)	(0.08)	
4	OFHC Cu	1.249	27.16	8.928	10.241	10.28	0.4%
		(0.002)	(0.06)	(0.003)	(0.006)	(0.08)	

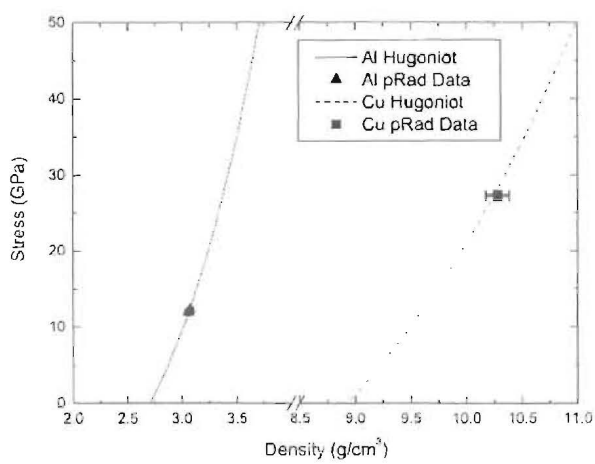

Figure 1: Results of proof-of-principle experiments, demonstrating <1% density reconstructions from dynamic proton radiography experiments.

Since that time further experiments have been performed studying material equation of state, focusing on solid-solid phase transitions. Figure 2 shows results from the alpha-epsilon phase transition in iron. The driving pressure of this experiment was designed to split the shock and phase transition waves, resulting in the two-wave structure shown in these radiographs. These results have been presented at various conferences and seminars and follow on work is being performed in 2009 for publication in early 2010.

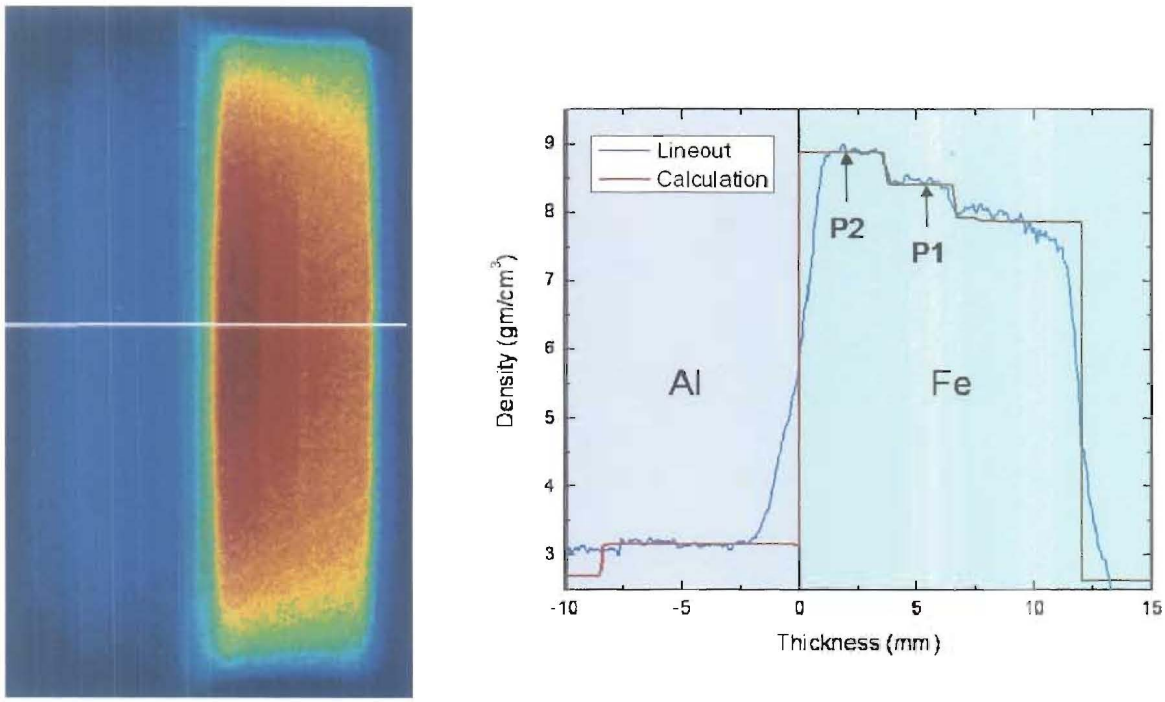

Figure 2: Left, color enhanced density distribution (red being the highest density) from a radiograph of an iron cylinder driven by an aluminum flyer, which was traveling from left to right. The leading density jump is the P1 wave and the second density jump is the phase transition or the P2 wave. Right: a lineout through the density distribution showing the agreement between model simulations and the radiographic density reconstructions.

The work described above has focused on equation of state measurements on materials driven by a supported shock. More recently experiments have been performed to investigate the potential for measuring equation of state in materials driven by high explosives with the goal of identifying solid-solid and solid-liquid phase boundaries. Because of the high resolution and multiple pulse capability of 800 MeV proton radiography the average shock velocity between radiographic frames and the density behind the shock discontinuity can be measured simultaneously. In an HE driven sample the shock pressure decreases as it traverses the sample, allowing for multiple measurements of points along the Hugoniot. A demonstration experiment has been performed using this technique. In this case a cylinder high explosives was used to drive a Taylor wave shock into a tin sample. The series of radiographs from these experiments are shown in figure 3, along with the points along the Hugoniot determined through density measurements and shock velocity measurements from the multiple time radiographs.

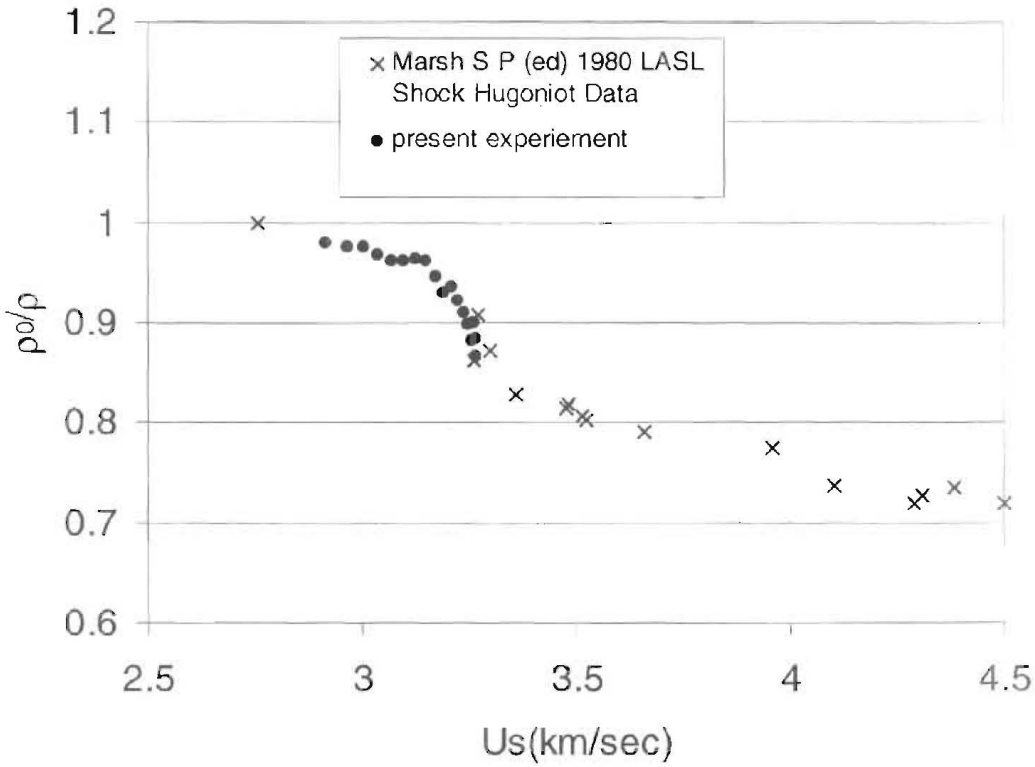

Figure 3: Top: multiple time radiographs of a HE driven shock traversing a tin sample. The shock velocity between each radiograph as calculated from a measurement of the leading edge of the shock and the inter-frame spacing of the radiographs. The density was inferred from the transmission of the radiographs.

The development of these techniques is being refined on known materials in preparation for experiments on materials with unknown properties. Successful development of this technique will result in a single experiment mapping out the Hugoniot from the peak pressure attainable with high explosives all the way down to nearly sound wave velocities.

5. High explosive dynamic material behavior:
Corner Turner Experiments, PI: Eric Ferm, EHT-H, Hydrodynamics

Proton radiographs show measurable changes in high explosive burn behavior as a function of HE type, lot, and temperature. For example, these variables impact the size of dead zones, or regions of unburned explosives. The corner turner experiments were designed to show dead zone regions caused by forcing a cylinder of HE to ignite a larger cylinder. A series of experiments show changes in the dead zone size with both temperature and lot. Figure shows one such experiment, where the formation of dead zones can be studied with time resolution. These results are used to validate HE burn models in ASC codes. Accurate measurement of the size and shape of the dead zones has only been achievable using proton radiography, and these data have proven to be invaluable for validating calculations.

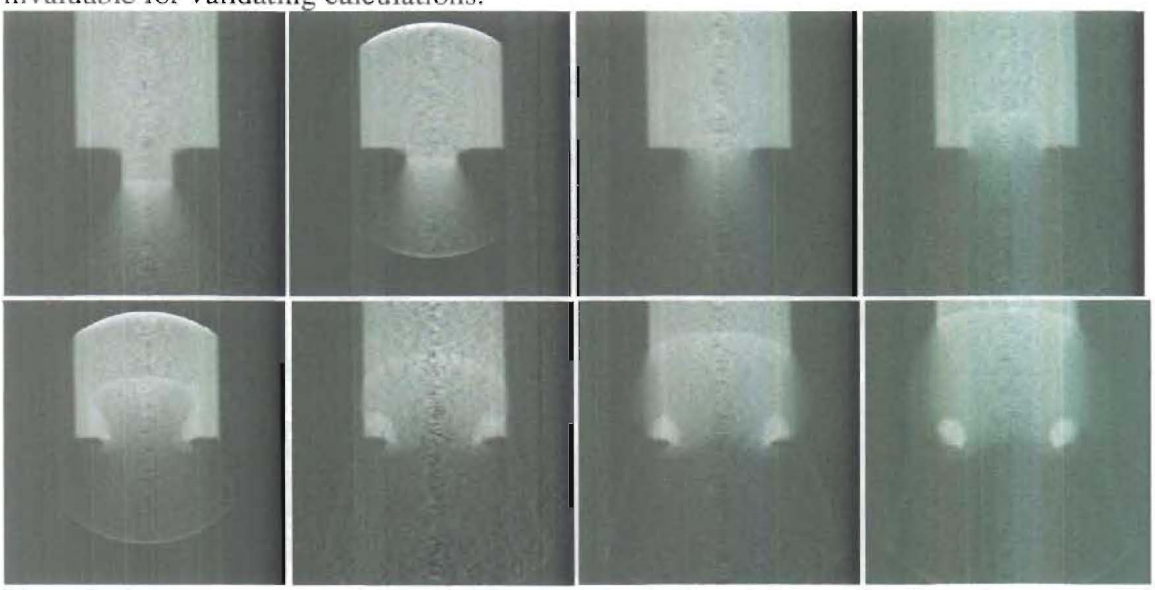

Figure 1. Corner turner experiment showing the propagation of the reaction front through an HE cylinder into a larger-diameter cylinder. Dead zones are visible as bright spots.

6. High Explosive Equation of State
Wave Collider Experiments, PI: Eric Ferm, EHT-H, Hydrodynamics; Calculations: Allen Mathews, X-4, Primary and Design Assessment.

In the wave collider experiment, two detonation waves collide, pass through each other, and continue to propagate through the HE detonation products. At the instant they collide, the pressure is higher than the Chapman-Jouget (CJ) pressure, and the experiment offers the possibility of testing the performance of EOS models in the pressure region above CJ and at rapidly changing densities.

The experimental setup of traditional HE-EOS cylinder tests differs from the wave collider experiment in that it consists of a thin copper pipe filled with HE that is detonated at only one end. The maximum steady pressure produced by the detonation wave in the cylinder test is called the CJ pressure. The JWL EOS is therefore only calibrated for pressures up to the CJ pressure, but not greater. The JWL EOS is frequently used in hydrodynamic modeling of HE detonation even though its failure to reproduce

experimental results at pressures above CJ has been documented extensively [4,5,6]. The second EOS for HE detonation products considered in this study is the one recently proposed by Davis [7]. The Davis gas EOS was calibrated so that it would reproduce experimental data that included pressures above CJ.

The parameters in the hydrocode models were varied systematically in order to match the pRad experimental data to corresponding simulations. The experimental data consisted of multiple time-frame images from a pRad data set that were captured in an HE collider sequence. The comparison between the experimental data and the simulation, Figure , 2 provides a means for validating hydrodynamic simulations at more than one time, thus adding more stringent constraints to the time evolution of explosively-driven processes. We applied the process to both JWL and Davis gas EOS models, and the results for the two models were almost indistinguishable in the density profiles. However, the two models did show differences in peak pressures at comparable times, as was expected. We are in the process of studying the effect of other parameter changes on differences in the profile and the shape of the shock-wave front. (citation of report "Analysis of Multiframe Proton Radiograph (PRAD) Images from HE Collider Experiments," Allen Mathews (X-4), Holmann Brand (X-7), and Kevin Buescher (X-8) LA-UR-03-3425)

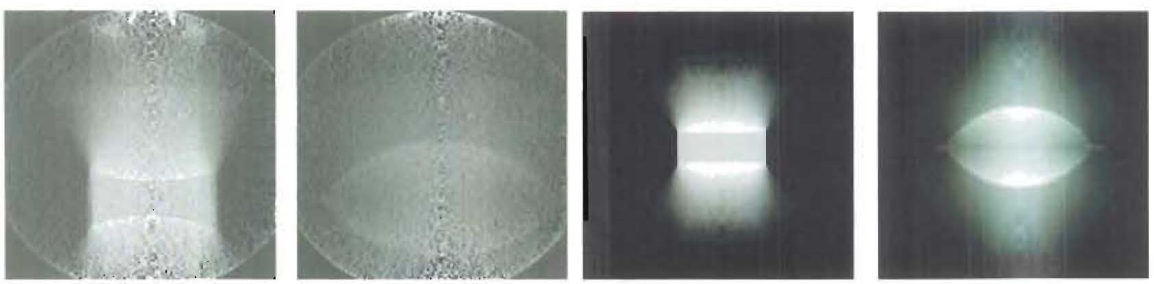

Figure 2: Two pRad images from the wave collider experiment (left), and two computational images at the same times (right). Simultaneous detonations occur at the top and bottom of each image, outside of the field of view. The left image was made shortly before the initial burn fronts collided (approximately 6.8 μs after the HE detonation). The right image shows the shock wave propagating through burned the HE (approximately 13.3 μs after the HE detonation). The waves collided at 7.8 μs. The experimental images show Abel inversion reconstructions from the original radiographs. Variations in the density of the burned HE in the simulations are the result of interactions between HE regions detonated at multiple points.

3. High Strain Rate Strength:

High Strain Rate Strength experiments, PI: Russ Olson, P-23, Neutron Science and Technology Group

The hydrodynamic simulation of explosively driven metals requires the inclusion of material strength. Some simulations employ a strain-rate independent model, such as Steinberg-Guinan (SG) strength model. More sophisticated simulations, such as the Preston, Tonks and Wallace (PTW) model include strain rate dependence. Typically the parameters for these models are determined at low strain rate from the interpretation of Hopkinson-Bar experiments and the strength model is then used to extrapolate through many orders of magnitude to predict material strength at high strain-rate. Figure 1 shows the Hopkinson-Bar data with the PTW model predictions overlaid
To understand the accuracy of this extrapolation a series of dynamic experiments have

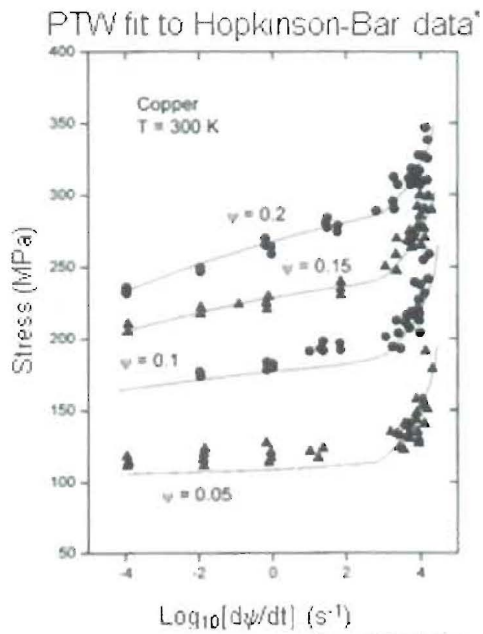

Figure 7: Low strain rate stress measurements compared to PTW fit to this data. This model and these fit parameters are typically then used for hydrodynamic simulations to predict material properties at strain rates orders of magnitude higher.

been performed at the proton radiography facility in collaboration with Russ Olson of LANL and Mary Jane Lindquist of LLNL. Figure 2 shows a schematic of the experimental layout. In these experiments expanding high explosives detonation products are used to shocklessly accelerate a metal sample, which has been machined to have a sinusoidal surface profile, to seed the Rayleigh-Taylor instability growth. The Rayleigh-Taylor growth rate, as measured via the multiple time radiography, is then used to compare to model predictions. These experiments have been performed to study the high strain rate strength properties of copper as a function of fabrication and preparation treatments (such as annealing and pre-straining). In addition these experiments were performed to study high strain rate strength in vanadium, tantalum and uranium to study the effects of crystalline structure on material strength. Figure 3 shows preliminary proton radiography growth data compared to SG and PTW predictions. All models

predicted strength inhibited growth after 9 μs, while the measurements show no sign of reduced growth rate.

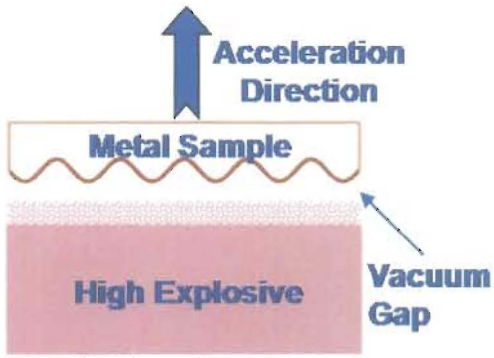

Figure 8: Schematic layout of high strain rate strength measurements performed at pRad.

These experiments are being carried out to verify existing strength models as well as develop the next generation of strength models by staff at LANL, LLNL, AWE and VNIIEF.

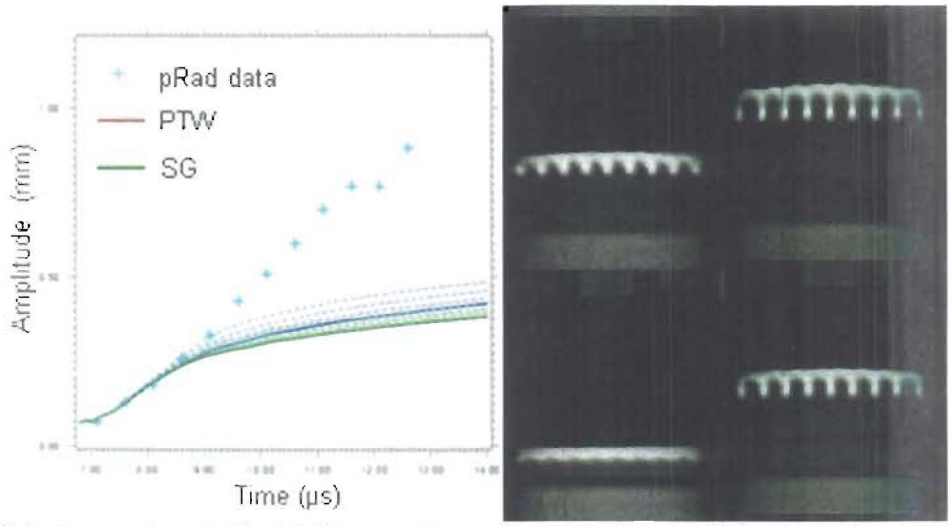

Figure 9: Left, experimental instability growth as a function of time. Right, dynamic radiography used to measure growth rate.

Once the theoretical and modeling capability has been established experiments similar to these will be proposed to study the strength characteristics of plutonium. These experiments will be proposed for execution at pRad or U1A.

3. RMI Instability Growth:
PI: William Buttler, P-23, Neutron Science and Technology Group

LANL is presently engaged in developing models of ejecta formation and transport for integration into LANL hydrodynamic simulations. It is believed that the underlying theory for ejecta formation is through Richtmyer-Meshkov instability growth of shocked rough surfaces. A series of proton radiography experiments have been performed to study Richtmyer-Meshkov instability growth of the resulting "bubbles and spikes" as well as studying the transport and breakup of these materials into vacuum and gas. The proton radiography data set, along with data collected at other facilities, is guiding the development of the LANL ejecta model, which will ultimately be implemented into the LANL hydrodynamic simulation codes.

Figure 1 shows the radiographic results from a pRad experiment performed in late 2008. This experiment was performed to study Richtmyer-Meshkov instability growth of shock liquefied tin xenon at an ambient pressure of 5 bar. A second experiment was also performed to study the Richtmyer-Meshkov instability growth into vacuum to study the differences in bubble and spike transport. Follow on experiment s have been executed in 2009 to study RMI growth, ejecta formation and transport when generated by Taylor wave and supported shocks into vacuum and high pressure gas.
The present state of this research is described by Buttler et al. in LA-UR-08-6293.

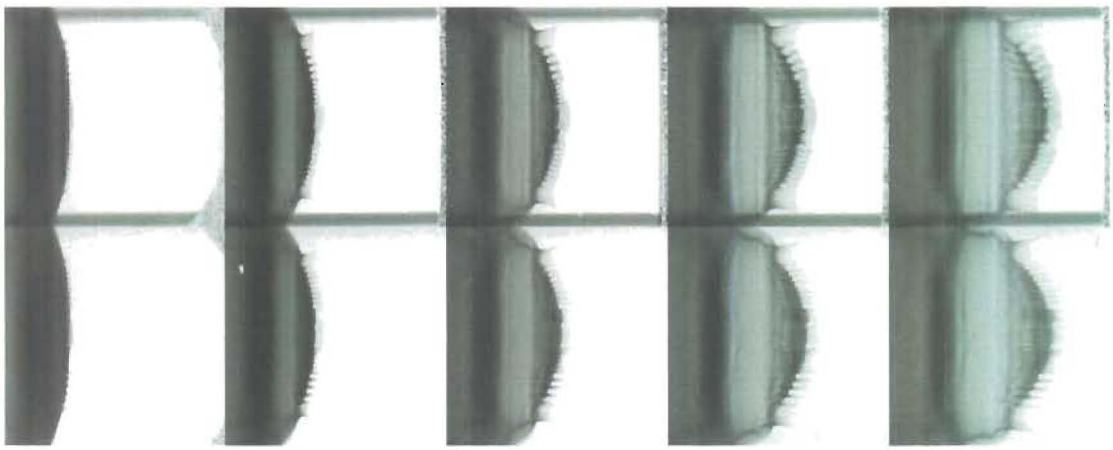

Figure 1: Comparison of ejecta formation and transport of liquefied tin in 5 bar of xenon (top) and into vacuum (bottom)

3. Plutonium Preparatory Experiments:
PI: Nick King, P-23, Neutron Science and Technology Group

The Bacchus series of experiment was designed to study plutonium strength characteristics. These experiments were designed to use small quantities of plutonium (<11 grams) driven by small quantities of high explosives (<30 grams TNT equivalent). These design restrictions would allow the experiment to be fired in Area C at LANSCE under the authorization basis which was approved in April, 2009.

In order to protect Area C from plutonium contamination these experiments will be executed within a confinement vessel which will be installed into a secondary confinement vessel. The design of the inner confinement vessel required some data on the fragment distribution within the inner confinement vessel. In addition the experimental technique of fielding these small scale experiments in two layers of confinement required testing before fabricating the final inner vessel system. Two experiments were fired to meet these two goals. The first was the fragment test and the multiple time radiographs from this experiment is shown in figure 1. The multiple time radiographs fired from the second experiment, fired with a lead sample, is shown figure 2.

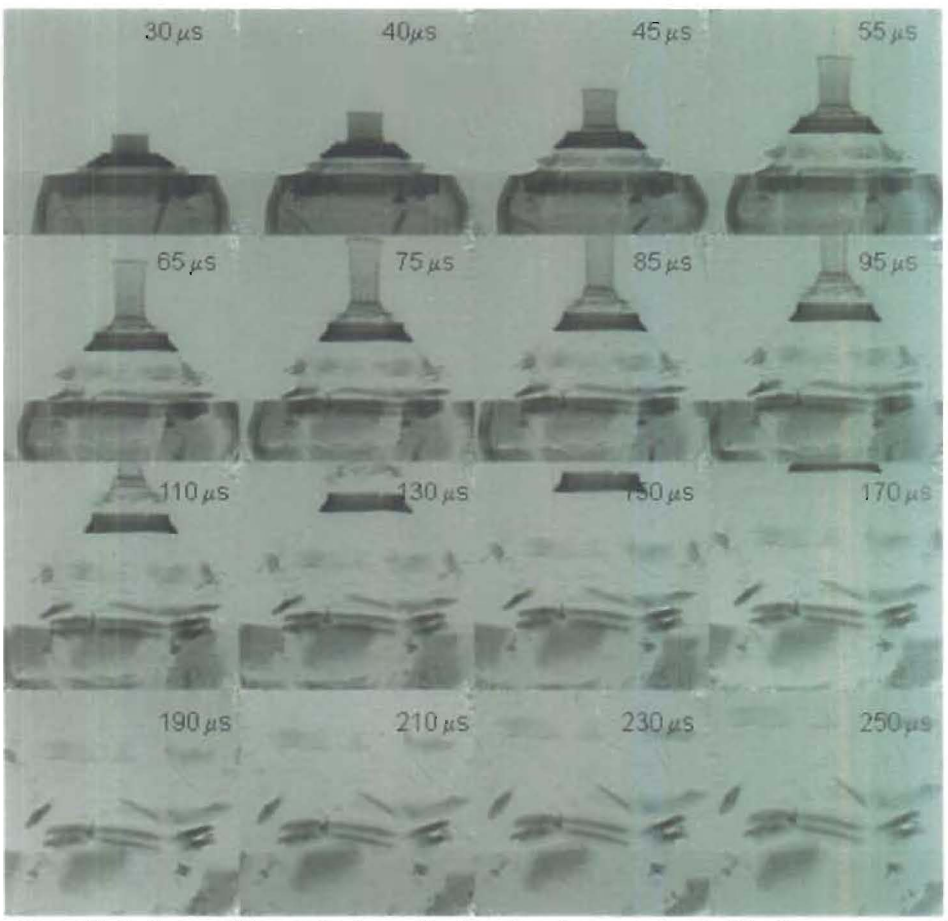

Figure 1: multiple time radiographs from the Bacchus fragment test. The fragment spatial and velocity distribution was used by vessel designers to guide and assess the design of the inner confinement vessel.

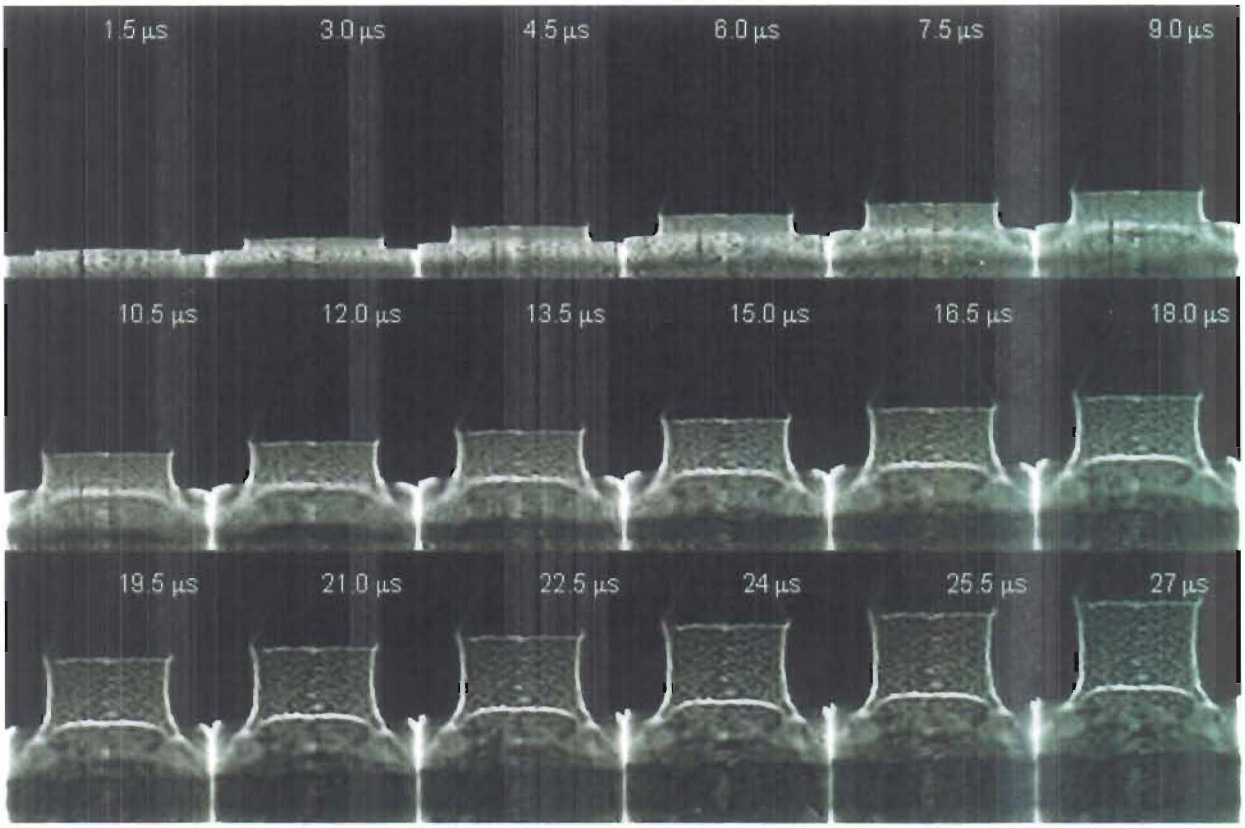

Figure 2: Multiple tie radiographs of the Bacchus radiographic test experiment. The results of this experiment demonstrated the capability of 800 MeV proton radiography to provide multiple time radiographs with sufficient resolution to meet the requirements of the Bacchus experiment.